Impact of CP Violation on $|V_{e3}|$

G. Couture, C. Hamzaoui and A.M. Lussier
Département des Sciences de la Terre et de l'Atmosphère,
Université du Québec à Montréal
C.P. 8888, Succ. Centre-Ville
Montréal, H3C 3P8

Abstract

We study the impact of the positivity of the measure of CP violation in neutrino oscillations on the values of $|V_{e3}|$ and $|V_{\mu 1}|$. We use the available information on the solar and atmospheric mixing parameters $|V_{e2}|$ and $|V_{\mu 3}|$ provided by neutrino oscillation data. We conclude that large values of $|V_{e3}|$ are preferred at 95% confidence level. This, in turn, favours large values for J_{lepton} compared to CP violation in the quark sector.

1 Introduction

There are now compelling observations that neutrinos (leptons) do mix like quarks and have non zero masses [1, 2, 3, 4, 5]. Therefore we have a mixing matrix, analogous to that of the quark sector. In the absence of a fundamental theory of the origin of mass, this matrix is parametrised by several indenpendant parameters. Clearly, one of the important goals of particle physics in the next years will be to determine these parameters with the highest precision possible. One hopes that the knowledge of this matrix will point the way to a more fundamental theory of lepton mixings. Lepton mixing also has far reaching consequences in leptogenesis [6] and in baryogenesis [7].

Over the last few years, several groups have strived to set bounds on the mixing parameters of the leptonic sector. Two preferred scenarios have emerged: the bi-maximal scenario [8] and the tri-bimaximal scenario [9]. All these scenarios are summarized in reference [10]. Recent data on neutrinos oscillations [11] favour the tri-bimaximal scenario of lepton mixing.

The purpose of this article is to study the role played by the measure of CP violation [12], namely J, in the structure of the leptonic mixing matrix [13]. A similar study has proven usefull before in the quark sector [14]. We will show that by using the positivity of J^2, it is possible to restrict the range of $|V_{e3}|^2$ and $|V_{\mu 1}|^2$ in a usefull way. As we will see shortly, the maximum amount of CP violation in neutrino oscillations is gauged by the value of $\sin\theta_{13}$ [15], which itself is closely related to $|V_{e3}|$. We will then concentrate on this last parameter and show that, at 95% confidence level (c.l.), $0.0065 \leq |V_{e3}|^2 \leq 0.05$.

In the next section, we will describe the parametrization that we used for our analysis, which we will explain in the third section. In the fourth and fifth sections we will present our results on $|V_{e3}|^2$ and $|V_{\mu 1}|^2$, and on J^2. We will conclude in the last section.

2 Rephasing Invariant Parametrization of the Mixing Matrix

We will assume that we have three neutrino flavors. In this case, the elements of the lepton mixing matrix are generally defined by

$$\begin{pmatrix} \nu_e \\ \nu_\mu \\ \nu_\tau \end{pmatrix} = \begin{pmatrix} V_{e1} & V_{e2} & V_{e3} \\ V_{\mu 1} & V_{\mu 2} & V_{\mu 3} \\ V_{\tau 1} & V_{\tau 2} & V_{\tau 3} \end{pmatrix} \begin{pmatrix} \nu_1 \\ \nu_2 \\ \nu_3 \end{pmatrix} \tag{1}$$

In terms of mixing angles, the mixing matrix becomes [11]

$$V_{PMNS} = UP = \begin{pmatrix} c_{12}s_{13} & s_{12}c_{13} & s_{13}e^{-i\delta} \\ -s_{12}c_{23} - c_{12}s_{23}s_{13}e^{i\delta} & c_{12}c_{23} - s_{12}s_{23}s_{13}e^{i\delta} & s_{23}c_{13} \\ s_{12}s_{23} - c_{12}c_{23}s_{13}e^{i\delta} & c_{12}s_{23} - c_{12}c_{23}s_{13}e^{i\delta} & c_{23}c_{13} \end{pmatrix} P \tag{2}$$

where U is a Cabibbo-Kobayashi-Maskawa like unitary matrix and CP-violation *à la Dirac* is implemented through the phase δ. P is a matrix that contains Majorana CP violating phases. These phases are not relevant to our analysis as long as we consider only the data from oscillation experiments [16]. Therefore, we can ignore them in what follows.

In order to describe CP-violation in neutrino oscillations, the mixing matrix V_{PMNS} can be parametrized in terms of four moduli [17]; we choose the following four independant moduli: $|V_{e2}|$, $|V_{e3}|$, $|V_{\mu 1}|$ and $|V_{\mu 3}|$.

As the V_{ij} are complex quantities, setting $V_{e3} = 0$ gives us two constraints: $|V_{e3}| = 0$ and $|V_{\mu 1}| = |V_{e2}|\sqrt{1-|V_{\mu 3}|^2}$. The whole mixing matrix is then described by $|V_{e2}|$ and $|V_{\mu 3}|$. Consequently, we have:

$$V_{PMNS} = \begin{pmatrix} \sqrt{1-|V_{e2}|^2} & |V_{e2}| & 0 \\ -|V_{e2}|\sqrt{1-|V_{\mu 3}|^2} & \sqrt{(1-|V_{e2}|^2)(1-|V_{\mu 3}|^2)} & |V_{\mu 3}| \\ |V_{e2}||V_{\mu 3}| & -|V_{\mu 3}|\sqrt{1-|V_{e2}|^2} & \sqrt{1-|V_{\mu 3}|^2} \end{pmatrix} \tag{3}$$

It is now possible to estimate the maximal value for $|V_{\mu 1}|$. In the bi-maximal scenario, one takes $|V_{\mu 3}| = |V_{e2}| = \frac{1}{\sqrt{2}}$ which leads to $|V_{\mu 1}|_{bi-max} = \frac{1}{2}$ and

$$U_{bi-max} = \begin{pmatrix} \frac{1}{\sqrt{2}} & \frac{1}{\sqrt{2}} & 0 \\ -\frac{1}{2} & \frac{1}{2} & \frac{1}{\sqrt{2}} \\ \frac{1}{2} & -\frac{1}{2} & \frac{1}{\sqrt{2}} \end{pmatrix} \tag{4}$$

In the tri-bimax scenario, one sets $|V_{e2}| = \frac{1}{\sqrt{3}}$ and $|V_{\mu 3}| = \frac{1}{\sqrt{2}}$. This leads to $|V_{\mu 1}|_{tri-bimax} = \frac{1}{\sqrt{6}}$ and

$$V_{tri-bimax} = \begin{pmatrix} \sqrt{\frac{2}{3}} & \frac{1}{\sqrt{3}} & 0 \\ -\frac{1}{\sqrt{6}} & \frac{1}{\sqrt{3}} & \frac{1}{\sqrt{2}} \\ \frac{1}{\sqrt{6}} & -\frac{1}{\sqrt{3}} & \frac{1}{\sqrt{2}} \end{pmatrix} \tag{5}$$

We argue that this maximal value of $|V_{\mu 1}|$ is quite reasonable as any non-zero value of V_{e3} will increase it or decrease it by an amount close to $|V_{e3}|$ or smaller [14, 17]. Nonetheless, we will study two cases later on: $|V_{\mu 1}|^2_{max} = 0.25$ and 0.35.
The exact expressions between the moduli of the elements of the mixing matrix (V_{PMNS}) and the mixing angles experimentally accessible, namely θ_{sun}, θ_{atm} and θ_{13}, can be found in Xing [10]; setting $|V_{e3}| = 0$ leads to $|V_{e2}| = sin\theta_{sun}$ and $|V_{\mu 3}| = sin\theta_{atm}$. The expressions that we need here are:

$$|V_{e3}|^2 = sin^2\theta_{13} \tag{6}$$
$$|V_{e2}|^2 = sin^2\theta_{12}\ cos^2\theta_{13} \tag{7}$$
$$|V_{\mu 3}|^2 = sin^2\theta_{23}\ cos^2\theta_{13} \tag{8}$$

Our current knowledge on the magnitude of the elements of the leptonic mixing matrix comes from experiments on neutrino oscillation and can be summarized as follows[18]:

$$\begin{aligned} \sin^2\theta_{12} &= 0.3 \pm 0.08 && (9)\\ \sin^2\theta_{23} &= 0.5 \pm 0.18 && (10)\\ \sin^2\theta_{13} &\leq 0.05 \ \text{ at } 3\sigma && (11) \end{aligned}$$

Note that these values are close to those of the tri-bimaximal scenario.

The measure of CP violation, J, is given in general as:

$$J = \Im m(V_{e2}V_{\mu 3}V_{e3}^*V_{\mu 2}^*) \tag{12}$$

It has been shown before that if any element of the mixing matrix goes to zero, CP violation *à la Dirac* vanishes [17]. However, the vanishing of CP violation does not imply that any element of the mixing matrix is zero.
From the previous expression for J, we can infer an upper bound:

$$|J| \leq |V_{e2}|\ |V_{\mu 3}|\ |V_{e3}|\ |V_{\mu 2}| \tag{13}$$

Using the values of the tri-bimaximal scenario ($|V_{e2}| = 1/\sqrt{3} = |V_{\mu 2}|,\ |V_{\mu 3}| = 1/\sqrt{2}$) we can get a rough estimate on the maximum value of $|J|$:

$$|J| \leq \frac{|V_{e3}|}{3\sqrt{2}} \tag{14}$$

Numerically, by taking the maximal value of $|V_{e3}| \sim \sqrt{0.05}$, we have $|J|_{max} \approx 0.05$

As can be seen from eqs. 1 and 2, $|V_{e3}|$ has the simplest relation to V_{PMNS} and CP violation. It is also a measure of the maximum amount of CP violation possible in the leptonic sector. We will therefore pay special attention to this parameter.
In terms of our 4 independant parameters, the measure of CP-violation is given by [17]

$$\begin{aligned} J^2 = (1 - |V_{e3}|^2 - |V_{e2}|^2)|V_{e3}|^2|V_{\mu 1}|^2|V_{\mu 3}|^2 \\ -\tfrac{1}{4}\left(|V_{e2}|^2 - |V_{\mu 1}|^2 + |V_{\mu 1}|^2|V_{e3}|^2 - |V_{\mu 3}|^2|V_{e3}|^2 - |V_{\mu 3}|^2|V_{e2}|^2\right)^2 \end{aligned} \tag{15}$$

3 Analysis

For our analysis, we use only the known mixing parameters: the solar mixing θ_{12}, the atmospheric mixing θ_{23}. We will use the positivity of J^2 to set an interval on $|V_{e3}|^2$ and $|V_{\mu 1}|^2$ consistent with data. In the following, we will assume that $cos^2\theta_{13} \approx 1$ and later on we will estimate how a variation in this value could affect our results. This means that we use $|V_{e2}|^2 \approx sin^2\theta_{12} = 0.3 \pm 0.08$ and $|V_{\mu 3}|^2 \approx sin^2\theta_{23} = 0.5 \pm 0.18$ and set the maximal value allowed for $|V_{\mu 1}|$ at that obtained from the bi-maximal scenario:

$$|V_{\mu 1}|_{max} = 0.5 \tag{16}$$

We performed our numerical analysis as follows. Using the central values for $|V_{e2}|^2$ and $|V_{\mu 3}|^2$ we use eq.-15 and require that J^2 be positive. This gives us a range of values for $|V_{e3}|^2$ and $|V_{\mu 1}|^2$, as can be seen on fig. 1: any combination within the parabola leads to a positive value of J^2. In order to take into account the uncertainties in $|V_{e2}|^2$ and $|V_{\mu 3}|^2$, we used a Monte Carlo method. We generated values for $|V_{e2}|^2$ and for $|V_{\mu 3}|^2$, independantly, according to the Gaussian distribution $exp[-0.5((x - x_c)/\sigma_x)^2]$ centered at x_c and with a standard deviation of σ_x. We covered the whole range from 0 to 0.6 for $|V_{e2}|^2$ and 0 to 1 for $|V_{\mu 3}|^2$ and verified that our distributions were centered at 0.3 and 0.5 with standard deviations of 0.08 and 0.18. For each combination of $|V_{e2}|^2$ and $|V_{\mu 3}|^2$, we compute a curve similar to that of fig. 1. The numbers that we present here were obtained from 50,000 such combinations of $(|V_{e2}|^2, |V_{\mu 3}|^2)$. Once we have these 50,000 curves, we scan the $|V_{e3}|^2 - |V_{\mu 1}|^2$ plane and count how many combinations of $(|V_{e2}|^2, |V_{\mu 3}|^2)$ allow a given point on the grid; we used a grid of 40,000 points (200 on each axis). If a point is allowed by the lower branch of a parabola, it gains a weight of 1, similarly for the upper branch of a parabola. If a point of the grid is rejected by a lower branch of a parabola, it looses a weight of 1; similarly for the upper branch of a parabola. This results in a given point of the grid gaining a weight of 2 if it is allowed by a parabola and gaining a weight of 0 if it is not allowed. This procedure leads to fig. 2-a where the probability of a given combination is given by the volume under the surface. The total volume under the surface is unity since we know that the final combination of parameters will be somewhere in our parameter space. The shape of this figure is easily understood: the base of the parabola will move a lot along the $|V_{\mu 1}|^2$ axis as values of $|V_{e2}|^2$ and $|V_{\mu 3}|^2$ are varied, thus excluding several points in the $|V_{e3}|^2 - |V_{\mu 1}|^2$ plane that are close to the $|V_{\mu 1}|^2$ axis, while points for larger values of $|V_{e3}|^2$ will be accepted by several parabolas. In order to put a confidence level on the combination $(|V_{e3}|^2, |V_{\mu 1}|^2)$, one simply slices the surface of fig. 2-a horizontally, starting from the top. Each slicing intersects the surface and the volume under the surface defined by this intersection represents the probability of finding the combinations $(|V_{e3}|^2, |V_{\mu 1}|^2)$. When this volume reaches 68% of the total volume, the curve that results of the intersection of the surface and the slicing is the 68% c.l. curve in the $|V_{e3}|^2$ and $|V_{\mu 1}|^2$ parameter space. The same applies for the 90% and 95% c.l. curves. This leads to figures 2-b.

In order to set c.l. limits on $|V_{e3}|^2$ alone, one has to integrate over $|V_{\mu 1}|^2$. Starting with fig. 2-a, it is easy to integrate over $|V_{\mu 1}|^2$: we simply add all the volume elements along an axis. This results in fig. 3, where the total surface under the curve is 1 since the physical, final parameter must be under this curve. In order to establish our c.l.s, we proceed as before and slice our figure horizontally, starting at the top. The intersection of our curve and the slicing, will define a certain range for $|V_{e3}|^2$ and when this range will cover a surface under the curve that represents 68% of the total surface, this range will be our 68% c.l. for $|V_{e3}|^2$. The same procedure applies for the 90% and 95% confidence level ranges.

4 Results

According to this procedure, we can say that the values of $|V_{e2}|^2 = 0.3 \pm 0.08$ and $|V_{\mu 3}|^2 = 0.5 \pm 0.18$ and the allowed ranges $0 \leq |V_{e3}|^2 \leq 0.05$ and $0 \leq |V_{\mu 1}|^2 \leq 0.25$ lead to a 68%, a 90%, and a 95% c.l. ranges in the $|V_{e3}|^2 - |V_{\mu 1}|^2$ parameter space as shown on figure 2-b. Globally, $|V_{\mu 1}|^2$ has to be larger than 0.027 at 95% c.l. and $|V_{e3}|^2$ has to be larger than 0.0017, also at 95% c.l.. These bounds become 0.034 and 0.0033, respectively, at 90% c.l.. If we intergrate over $|V_{\mu 1}|^2$, we can say the 68% c.l. range for $|V_{e3}|^2$ is 0.0228 – 0.05; the 90% c.l. range is 0.0103 – 0.05 and the 95% c.l. range is 0.0065 – 0.05. Therefore, we can say that values of $|V_{e3}|^2$ smaller than 0.0065 are excluded at the 95% c.l..

We can also project ourselves in the future and ask what these limits on $|V_{e3}|^2$, after integration over $|V_{\mu 1}|^2$, will become once the errors on $|V_{e2}|^2$ and $|V_{\mu 3}|^2$ will have been reduced. We performed the same analysis as above but we reduced the error on $|V_{e2}|^2$ and $|V_{\mu 3}|^2$ to 0.02 and 0.04, respectively. We studied 9 different combination of $|V_{e2}|^2$ and $|V_{\mu 3}|^2$: (0.22, 0.30, 0.38) $\times$ (0.32, 0.50, 0.68), respectively. The *bump* that appears on fig. 2-a moves substantially over the allowed ranges of $|V_{e3}|^2$ and $|V_{\mu 1}|^2$ but once we integrate over $|V_{\mu 1}|^2$ the allowed ranges of $|V_{e3}|^2$ change very little with the different combinations: 0.023 – 0.05 at 68% c.l., 0.011 – 0.05 at 90% c.l. and 0.0068 – 0.05 at 95% c.l. The only exception being (0.38, 0.50) where they are 0.021 – 0.05, 0.0093 – 0.05, and 0.0058 – 0.05.

One could ask how these bounds on $|V_{e3}|^2$ will vary if we allow the ranges on $|V_{e3}|^2$ and $|V_{\mu 1}|^2$ to vary. We explored this possibility and changed the ranges to $0 \leq |V_{e3}|^2 \leq 0.07$ and $0 \leq |V_{\mu 1}|^2 \leq 0.35$. From fig. 2-a, we can expect the general behaviour to continue for larger values of $|V_{e3}|^2$ and $|V_{\mu 1}|^2$. The different c.l. ranges obtained from the central experimental values of $|V_{e2}|^2$ and $|V_{\mu 3}|^2$ with their current errors, are shown on fig. 2-c. The different ranges are: 0.010 – 0.07 on $|V_{e3}|^2$ and 0.051 – 0.285 on $|V_{\mu 1}|^2$ at 68% c.l., 0.0025 – 0.07 on $|V_{e3}|^2$ and 0.021 – 0.333 on $|V_{\mu 1}|^2$ at 90% c.l., 0.0011 – 0.07 on $|V_{e3}|^2$ and 0.014 – 0.35 on $|V_{\mu 1}|^2$ at 95%. Furthermore, when we integrate over $|V_{\mu 1}|^2$, the c.l. ranges on $|V_{e3}|^2$ are 0.0322 – 0.07, 0.0147 – 0.07, and 0.0091 – 0.07, at 68%, 90%, and 95%, respectively. This strenghtens our statement that values of $|V_{e3}|^2$ smaller than 0.0065 are excluded at the 95% c.l..

In this context of larger bounds on $|V_{e3}|^2$ and $|V_{\mu 1}|^2$, we also projected ourselves in the future and redid the study with smaller errors on $|V_{e2}|^2$ and $|V_{\mu 3}|^2$, namely 0.02 and 0.04. The results are that, again the different c.l. limits are rather insensitive to the different combinations of $|V_{e2}|^2$ and $|V_{\mu 3}|^2$ used and read as follows: 0.033 – 0.07 at 68% c.l., 0.015 – 0.07 at 90% c.l. and 0.0095 – 0.07 at 95% c.l. The only exception being (0.38, 0.32) where they are 0.030 – 0.07, 0.014 – 0.07, and 0.0088 – 0.07.

5 What can we say about J^2 ?

At this point, one can ask what the typical values of J^2 in the allowed ranges are. On figure 4, we simply plot J^2 as a function of $|V_{e3}|^2$ and $|V_{\mu 1}|^2$ for $|V_{e2}|^2 = 0.3$ and $|V_{\mu 3}|^2 = 0.5$; the intersection of the *cone* with the plane is our fig. 1. On this figure, the maximum value of J^2 is 2.42×10^{-3}. One also sees that J^2 decreases rapidly as we move away from the peak. Note however that for the allowed ranges discussed previously, the values taken by J^2 will be typically larger than 3×10^{-4}. In order to give a better estimate, we generated combinations of our 4 parameters with the weights given by figure 2-a and calculated J^2 for each combination. The results are that for all our c.l. ranges, J^2 takes values between $\sim 3 \times 10^{-8}$ and 2.7×10^{-3} while the standard deviations of the distributions are constant at 0.6×10^{-3}. The average values of the distributions vary a little: 1.1×10^{-3} over the 68% confidence level range, 0.98×10^{-3} over the 90%, and 0.97×10^{-3} over the 95% cl range. Globally, these distributions do not vary much over our different c.l. ranges. Comparing figures 2-b-c with figure 1, it is clear that we cannot exclude $J^2 = 0$ since the boundaries between J^2 positive and negative are well within our confidence level ranges for many combinations of $|V_{e2}|^2$ and $|V_{\mu 3}|^2$. Our real minimal value is in fact zero and only numerical accuracy made it non-zero. What is important here is not the minimal value but rather the average values over the different domains: these are clearly far from zero and we can say that smaller values of J^2 are disfavoured.

As for J, the results are practically independant of the c.l. ranges and read as $J_{min} \sim 2 \times 10^{-4}$, $J_{max} = 0.05$, with an average value of 0.03 and a standard deviation of 0.01. The average values are the more meaningful results and small values are again strongly disfavoured. These are the strongest statements that we can make about J^2 and J.

From the previous variations on our parameters, it is clear that our initial approximation (*ie* $|V_{e2}|^2 \approx sin^2\theta_{12} = 0.3 \pm 0.08$ and $|V_{\mu 3}|^2 \approx sin^2\theta_{23} = 0.5 \pm 0.18$) has very little impact on our results.

6 Conclusion

The positivity of J^2 has proven a useful tool in setting constraints on different parameters of the leptonic mixing sector. Using only this variable, we can say that values of $|V_{e3}|^2$ smaller than 0.0065 are excluded at 95%, stronly disfavoured, by current data on $|V_{e2}|^2$

and $|V_{\mu 3}|^2$. Such large values are in fact preferred by some authors as they can help in establishing the complementarity relations between quark and lepton mixing [19]. From fig. 4, one sees that a large value of $|V_{e3}|^2$ is not a guarantee of CP violation but simply favours large CP violation.

We can also say that J^2 must be smaller than 2.7×10^{-3} and that values much smaller than 1×10^{-3} are strongly disfavoured. This translates into $J_{max} \approx 0.052$ and values much smaller than 0.03 being also strongly disfavoured. Such values of J_{lepton} are typically 1000 times larger than values of J_{quark}.

When looking at figures 1 and 2, one can see that the positivity of J^2 will not be able to exclude $|V_{e3}|^2 = 0$ since the parabola will always extend all the way down to $|V_{e3}|^2 = 0$, no matter what the experimental precision on $|V_{e2}|^2$ and $|V_{\mu 3}|^2$ is. All we can do is set some confidence limits.

Considering figures 1 and 4, it is clear that the tightest indirect contraints on $|V_{e3}|^2$ and $|V_{\mu 1}|^2$ will come from an upper limit or a direct measurement of CP violation in neutrino oscillations; from a limit or a direct measurement of J_{lepton}. This would reduce the space to a narrow strip following the parabola of fig. 1. Short of such a measurement, one will have to rely on independant measurement of $|V_{e3}|^2$ and $|V_{\mu 1}|^2$. A measurement of $|V_{\mu 1}|^2$ *far away* from 0.15 (assuming that $|V_{e2}|^2$ and $|V_{\mu 3}|^2$ keep their current central values) would lead to the smallest possible range on $|V_{e3}|^2$ and push it far from 0, thereby increasing the probability of large CP violation. Similarly, a measurement of $|V_{e3}|^2$ with a very small value would put the tightest limits on $|V_{\mu 1}|^2$ and at the same time would reduce greatly the possibility of large value of $|J|^2$. Assuming that a small value of $|V_{e3}|^2$ will be difficult to measure, one concludes that experimental efforts should be devoted to measuring $|V_{\mu 1}|^2$ since this could potentially strongly restrict the range of $|V_{e3}|^2$. Let's not forget that complete determination of the neutrino mixing matrix will shed some light on the deep structure of the leptonic spectrum and help us understand better the properties of neutrinos and mass generation in general.

7 Acknowldgements

It is a pleasure to thank Dr. G. Azuelos for suggesting the use of Monte Carlo methods. This work was supported in part by NSERC of Canada.

References

[1] Super-KamioKaNDE Collaboration, Y. Fukuda et al., Phys. Lett. B **436**, 33 (1998); Phys. Rev. Lett. **81**, 1562 (1998).

[2] SNO Collaboration, Q. R. Ahmad et al., Phys. Rev. Lett. **89**, 011301 (2002); Phys. Rev. Lett. **89**, 011302 (2002).

[3] KamLAND Collaboration, K. Eguchi et al., Phys. Rev. Lett. **90**, 021802 (2003).

[4] K2K Collaboration, M. H. Ahn et al., Phys. Rev. Lett. **90**, 041801 (2003).

[5] CHOOZ Collaboration, M. Apollonio et al., Phys. Lett. B **420**, 397 (1998); Palo Verde Collaboration, F. Boehm et al, Phys. Rev. Lett. **84**, 3764 (2000).

[6] M. Fukutia and T. Yanagida, Phys. Lett. B**174**, 45 (1986); P. Langacker, P.D. Peccei and T. Yanagida, Mod. Phys. Lett. A**1**, 541 (1986); M. Luty, Phys. Rev. D**45**, 455 (1992); R.N. Mohapatra and X. Zhang, Phys. Rev. D**46**, 5331 (1992); G. Giudice et al., Nucl. Phys. B**686**, 89 (2004); A. Pilaftsis and T. Underwood, Nucl. Phys. **692**, 303 (2004); W. Buchmuller, P. Di Bari and M. Plumacher, Nucl. Phys. B**665**, 445 (2003); H. B. Nielsen and Y. Takanishi, Phys. Lett. B**507**, 241 (2001); W. Buchmuller, R. D. Peccei and T. Yanagida, hep-ph/0502169 (2005).

[7] A. D. Dolgov, hep-ph/9707419; V. A. Rubakov and M. E. Shaposhnikov, Usp. Fiz. Nauk **166**, 493 (1996) [Phys. Usp. **39**, 461 (1996)]; A. Riotto and M. Trodden, Ann. Rev. Nucl. Part. Sci. **49**, 35 (1999).

[8] W. Rodejohann, Phys. Rev. D**69**, 033005 (2004); Nucl. Phys. B**687**, 31 (2004); C. Giunti and M. Tanimoto, Phys. Rev. D**66**, 053013 (2002); Phys. Rev. D**66**, 113006 (2002); N. Li and B.-Q. Ma, Phys. Lett. B**600**, 248 (2004).

[9] L. Wolfenstein, Phys. Rev. D**18**, 958 (1978); P. F. Harrison, D. H. Perkins, and W. G. Scott, Phys. Lett. B**530**, 167 (2002); Z.Z. Xing, Phys. Lett. B**533**, 85 (2002); X.G. He and A. Zee, Phys. Lett. B**560**, 87 (2003); C.I. Low and R.R. Volkas, Phys. Rev D**68**, 033007 (2003); A. Zee, Phys. Rev. D**68**, 093002 (20023); G. Altarelli, F. Feruglio, hep-ph/0504165 (2005).

[10] Z.Z. Xing, Int. J. Mod. Phys. A **19** (2004) 1 and references therein.

[11] Particle Data Group, S. Eidelman et al., Phys. Lett. B**592**, 1 (2004).

[12] C. Jarlskog, Phys. Rev. Lett. **55**, 1039 (1985); I. Dunietz, O. W. Greenberg and D.-d. Wu, Phys. Rev. Lett. **55**, 2935 (1985); C. Hamzaoui and A. Barroso, Phys. Lett. B**154**, (1985) 202.

[13] B. Pontecorvo, Zh. Eksp. Teor. Fiz. **33**, 549 (1957) [Sov. Phys. JETP **6**, 429 (1957)]; Zh. Eksp. Teor. Fiz. **34**, 247 (1957) [Sov. Phys. JETP **7** 172 (1958)]; Z. Maki, M. Nakagawa and S. Sakata, Prog. Theor. Phys. **28** 870 (1962).

[14] G. Bélanger, C. Hamzaoui and Y. Koide, Physical Review **D45** (1992) 4186; G. Bélanger, E. Boridy, C. Hamzaoui and G. Jakimow, Physical Review **D48** (1993) 4275.

[15] M. Fukugita and M. Tanimoto, Phys. Lett. B **515**, 30 (2001); M. Frigerio and A.Yu. Smirnov, Nucl. Phys. B **640** (2002) 233; Phys. Rev. D **67** (2003) 013007; S.F. King, in Proceedings of 10th International Workshop on Neutrino Telescopes edited by M. Baldo-Ceolin (U. of Padua Publication, Italy, 2003), Neutrino Mass, Flavor and CP Violation, [arXive:hep-ph/0306095]; Z.Z. Xing, Int. J. Mod. Phys. A **19** (2004) 1; O.L.G. Peres and A.Yu. Smirnov, Nucl. Phys. B **680** (2004) 479; C.H. Albright, Phys. Lett. B **599** (2004) 285; J. Ferrandis and S. Pakvasa, Phys. Lett. B **603** (2004) 184; S. Zhou and Z.Z. Xing, Euro. Phys. J. C **38** (2005) 495; S.T. Petcov and W. Rodejohann, Phys. Rev. D **71** (2005) 073002; G.C. Branco and M.N. Rebelo, New. J. Phys. **7** (2005) 86; C. Jarlskog, Phs. Lett. B**609** (2005) 323; S.T.Petcov. Nucl. Phys. Proc. Suppl. **143** (2005) 159; A. Datta, L. Everett and P. Ramond, hep-ph/0503222.

[16] G.C. Branco and M.N. Rebelo, New. J. Phys. **7** (2005) 86.

[17] C. Hamzaoui, Physical Review Letter **61**, 35 (1988); C. Hamzaoui, *A Geometrical Parametrization of the Quark Mixing Matrix*, in Proceedings of the Rare Decay Symposium, Vancouver, Canada, november 30 - december 3, 1988, TRIUMF, edited by D. Bryman, J. Ng, R. Numao, J. Poutissou, p. 469; A. Campa, C. Hamzaoui and V. Rahal, Physical Review **D39**, 3435 (1989).

[18] For recent reviews, see J. N. Bahcall, M. C. Gonzalez-Garcia and C. Pena-Garay, JHEP **0408**, 016 (2004) [arXiv: hep-ph/0406294]; C. Gonzalez-Garcia and M. Maltoni, hep-ph/0406056; M. Maltoni, T. Schwetz, M. Tortola and J. W. F. Valle, hep-ph/0405172; A. Strumia, F. Vissani, hep-ph/0503246.

[19] J. Ferrandis and S. Pakvasa, hep-ph/0412038; S. Pakvasa, hep-ph/0502012; S. Antusch, S. F. King and R. N. Mohapatra, hep-ph/0504007; R. N. Mohapatra, hep-ph/0504138;

8 Figures Captions

Figure 1: Limits in the $|V_{e3}|^2 - |V_{\mu 1}|^2$ plane obtained from the positivity of J^2. The parabola represents $J^2 = 0$; the space inside represents positive values of J^2.
Figure 2-a: Probability distribution in the $|V_{e3}|^2 - |V_{\mu 1}|^2$ plane obtained from 50,000 curves similar to those of figure 1. The vertical axis is in arbitrary units as the volume under the curve, representing the total probability, is unity.
Figure 2-b: Confidence levels obtained from figure 2-a. The 68% c.l. has the smallest surface while the 95% c.l. has the largest.
Figure 2-c: Similar to figure 2-b but with $0 \leq |V_{e3}|^2 \leq 0.07$ and $0 \leq |V_{\mu 1}|^2 \leq 0.35$.
Figure 3: Probability distribution of $|V_{e3}|^2$ after integrating the $|V_{\mu 1}|^2$ axis of figure 2-a.
Figure 4: J^2 for different values of $|V_{e3}|^2$ and $|V_{\mu 1}|^2$ using $|V_{e2}|^2 = 0.3$ and $|V_{\mu 3}|^2 = 0.5$

Fig.1

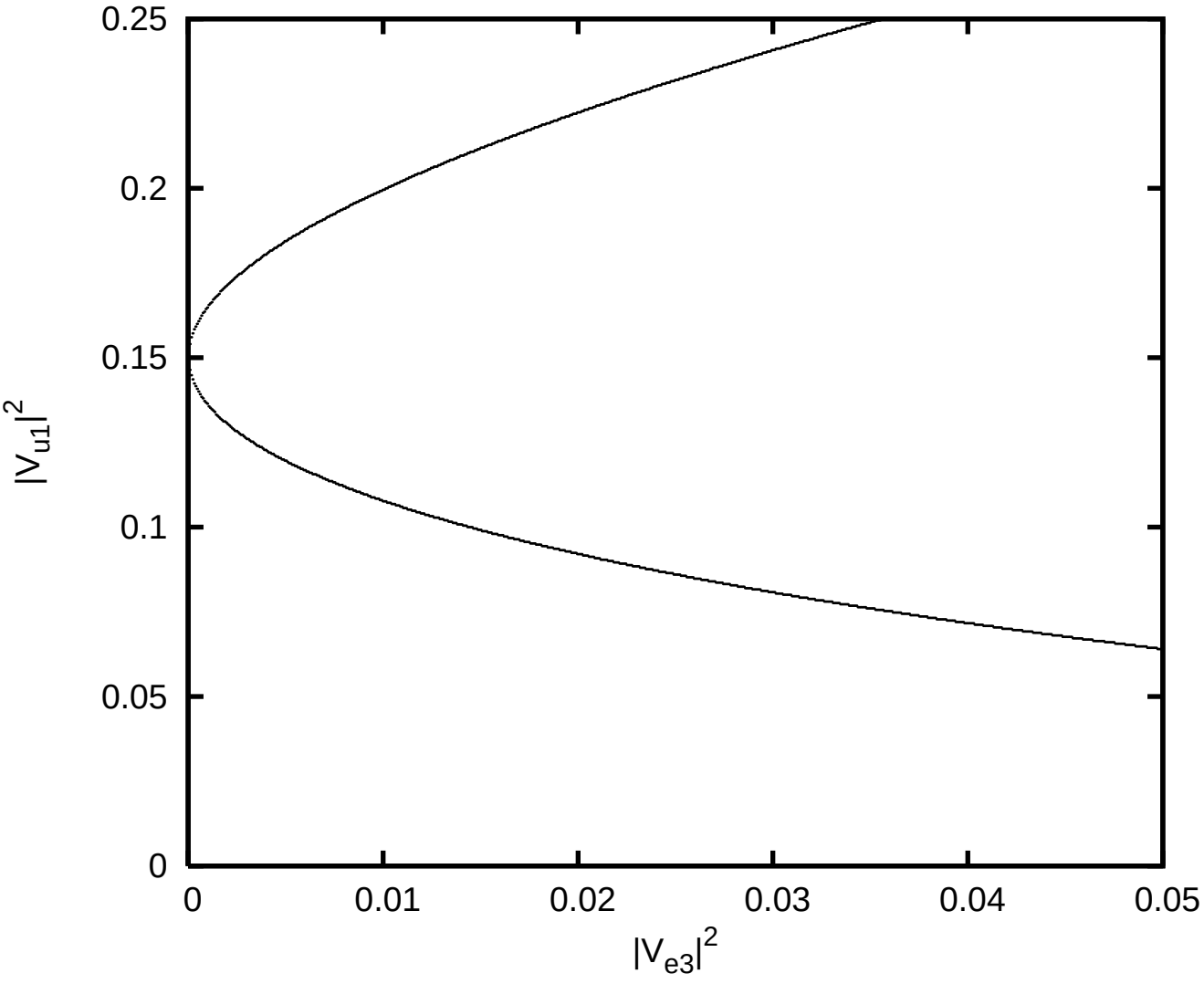

Fig. 2-a

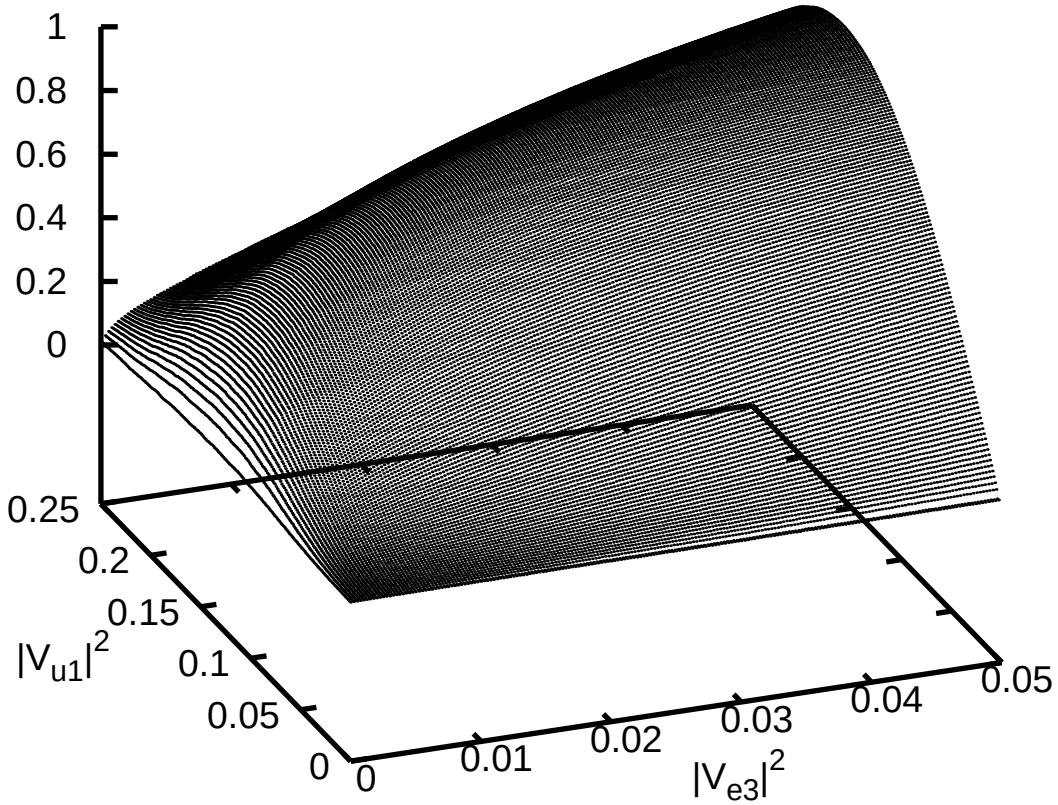

Fig. 2-b

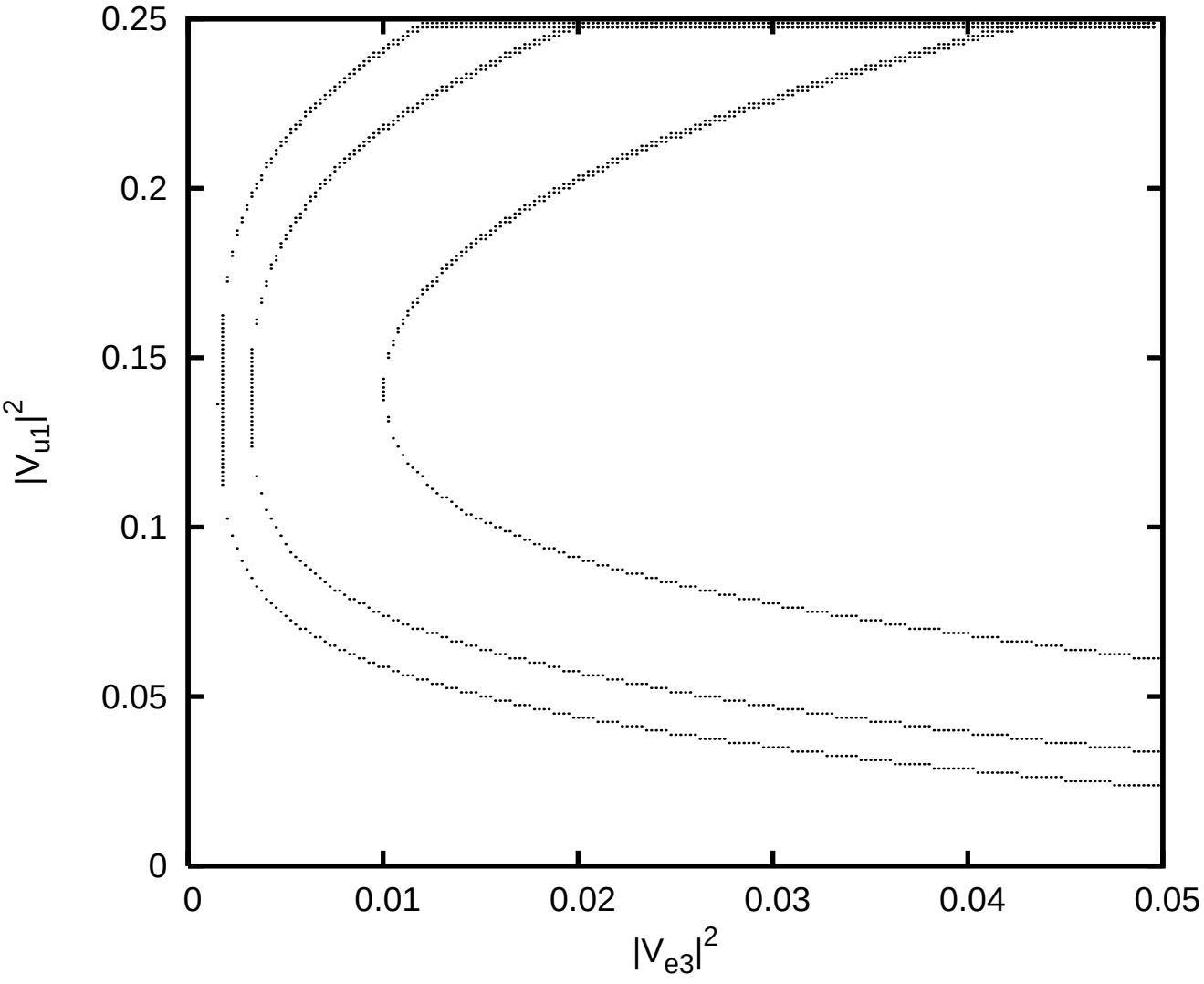

Fig. 2-c

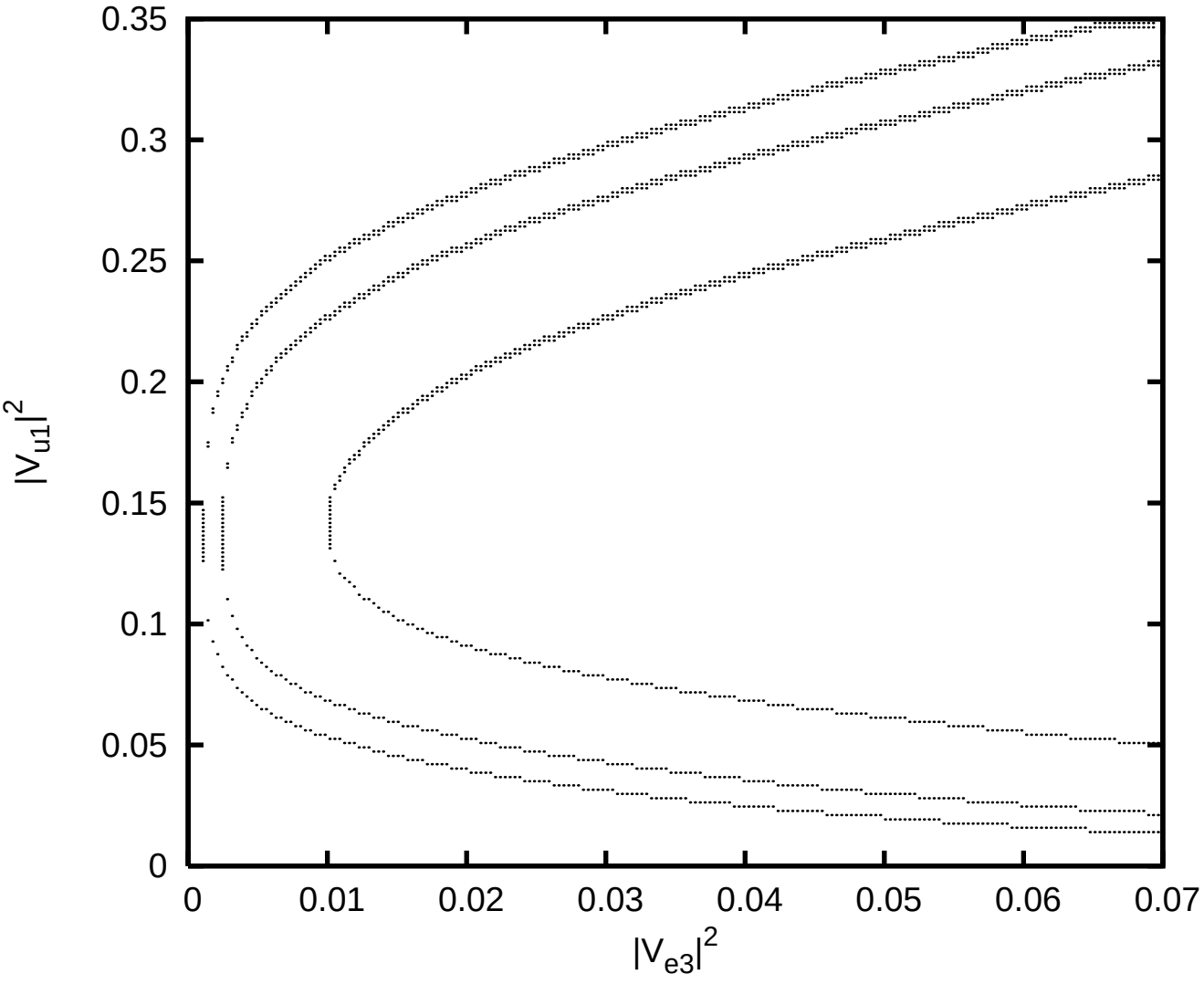

Fig. 3

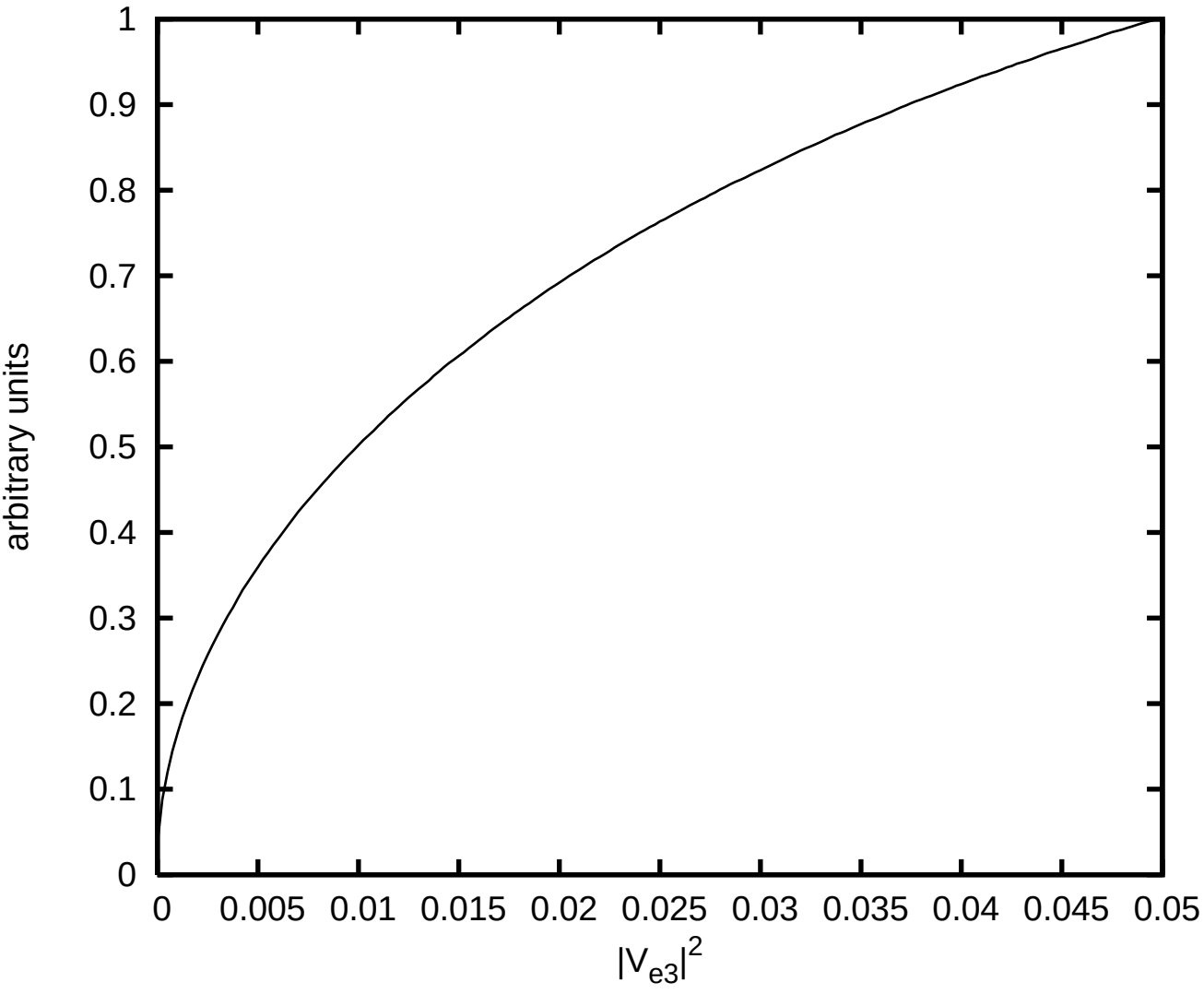
arbitrary units
1
0.9
0.8
0.7
0.6
0.5
0.4
0.3
0.2
0.1
0
0
0.005
0.01
0.015
0.02
0.025
0.03
0.035
0.04
0.045
0.05
$|V_{e3}|^2$

Fig. 4

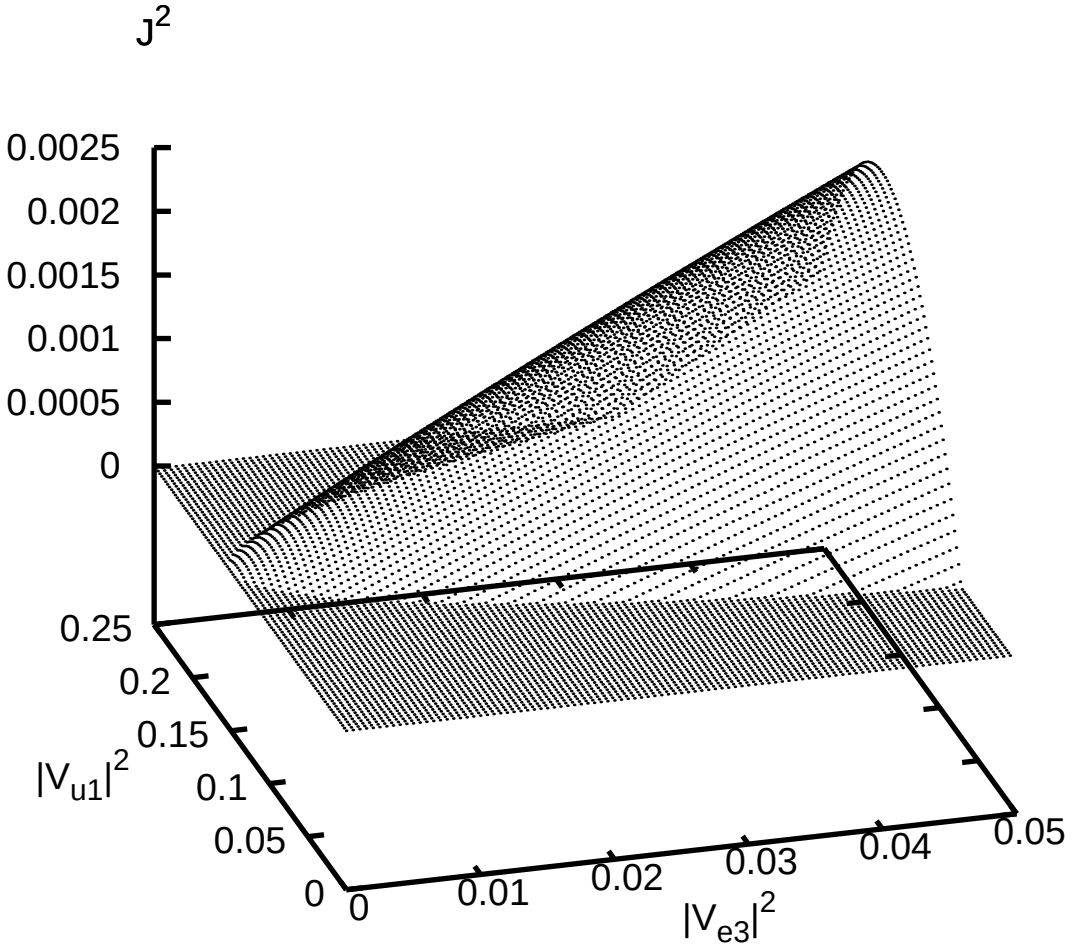
J^2
0.0025
0.002
0.0015
0.001
0.0005
0
0.25
0.2
0.15
0.1
0.05
0
|V_u1|^2
0
0.01
0.02
0.03
0.04
0.05
|V_e3|^2